Mucus from human bronchial epithelial cultures: rheology and adhesion across length scales

Myriam Jory, Dario Donnarumma, Christophe Blanc, Karim Bellouma, Aurélie Fort, Isabelle Vachier, Laura Casanellas, Arnaud Bourdin, Gladys Massiera

Mucus from human bronchial epithelial cultures: rheology and adhesion across length scales

Myriam Jory[1], Dario Donnarumma[1], Christophe Blanc[1], Karim Bellouma[1], Aurélie Fort[2,3], Isabelle Vachier[2,3], Laura Casanellas[1], Arnaud Bourdin[2] and Gladys Massiera[1]

[1]Laboratoire Charles Coulomb, Université de Montpellier and CNRS UMR 5221, 34095 Montpellier, France
[2]Inserm U1046, Université de Montpellier, Respiratory Disease, CHU Montpellier, 34295 Montpellier, France
[3]Médecine Biologie Méditerranée, Montpellier, France

Mucus is a viscoelastic aqueous fluid that participates in the protective barrier of many mammals' epithelia. In the airways, together with cilia beating, mucus rheological properties are crucial for lung mucociliary function, and, when impaired, potentially participate in the onset and progression of chronic obstructive pulmonary disease (COPD). Samples of human mucus collected *in vivo* are inherently contaminated and are thus poorly characterized. Human bronchial epithelium (HBE) cultures, differentiated from primary cells at an air–liquid interface, are highly reliable models to assess non-contaminated mucus. In this paper, the viscoelastic properties of HBE mucus derived from healthy subjects, patients with COPD and from smokers are measured. Hallmarks of shear-thinning and elasticity are obtained at the macroscale, whereas at the microscale mucus appears as a heterogeneous medium showing an almost Newtonian behaviour in some extended regions and an elastic behaviour close to boundaries. In addition, we developed an original method to probe mucus adhesion at the microscopic scale using optical tweezers. The measured adhesion forces and the comparison with mucus-simulants rheology as well as mucus imaging collectively support a structure composed of a network of elastic adhesive filaments with a large mesh size, embedded in a very soft gel.

Subject Areas:
biomaterials, biophysics

Keywords:
mucus, rheology, adhesion, hydrogel, polysaccharides, human bronchial epithelia

Author for correspondence:
Gladys Massiera
e-mail: gladys.massiera@umontpellier.fr

1. Introduction

Mucus is a viscoelastic sticky fluid coating mucosal surfaces and produced by epithelial secretory cells. It ensures hydration, lubrication and/or a protection barrier for many mammalian epithelia such as the respiratory, gastrointestinal and urogenital epithelia and for the ocular system. The composition, structure and physical properties of this hydrogel vary significantly among the different epithelia according to their dedicated functions. Whereas the mucus dry mass can be as high as 6.5% in thick cystic fibrosis samples, in non-pathological conditions, airways mucus is classically reported to contain approximately 98% of water and approximately 2% of salt and organic compounds, including anionic glycoproteins, mucins, which are the major functional components of mucus hydrogels. In bronchial epithelia, mucin concentration is approximately 0.2–1.0 wt% [1]. Mucins forming the hydrogel network are called gel-forming mucins (GFMs). Among them, MUC5AC and MUC5B are the most expressed in the airways. In aqueous solution, these high molecular weight proteins form a viscoelastic network by both covalent links and reversible interactions. In airway diseases, including chronic obstructive pulmonary disease (COPD), the mucus composition and its physical characteristics represent one of the most impacting patient reported outcomes [2] and have been shown to participate to disease progression [3].

Mucus viscoelastic and flowing properties play a key role in the efficiency of mucociliary clearance and also for drug and pathogen accessibility. The relationship between structure and rheology of these hydrogels has been investigated on mucus of various origins [4–7]. Filancemeter is the device which was originally used to characterize mucus spinnability [8,9], by probing mucus under an extensional deformation. Since shear is the dominant deformation in transport phenomena, mucus gels are nowadays more often characterized by the elastic and loss shear moduli related, respectively, to the energy stored and the energy dissipated in the gel. Rheology moduli reported in the literature span more than five orders of magnitude depending on the mucus origin and the way it was collected and assessed [10]. Nevertheless, most mucus gels share similar rheological characteristics. First, the elastic modulus is greater than the loss modulus and varies with frequency according to a power law with exponents smaller than 1 and often close to 0 [6,7,11–17]. Mucus flows more easily at higher shear rates and only above a critical applied stress [11,12,14,16,18]. Finally, whereas mucus exhibits the characteristics of a soft elastic and shear-thinning gel under a rheometer, elastic moduli measured at a microscopic scale are smaller in amplitude and have a different frequency dependence [7,13,18–20]. Using electron microscopy in most cases and more recently with high-resolution immunostaining in the hydrated state, the structure of mucus was shown to be highly heterogeneous [21] as a result of the various interactions between the mucins as reviewed elsewhere [4] and recently used to predict mucin self-assembly [22]. Based on the current knowledge on mucin assembly, and on existing imaging of mucus, several network structures have been proposed recently to explain the length scale dependent rheology of mucus gels. A foam-like structure [5,7] for mucus from horse lungs and a coupled two-fluid system [13] for a marine worm mucus were described. In this paper, we quantified, at different length scales, the viscoelastic properties of mucus collected from human bronchial epithelium (HBE) cultures by performing active micro- and macro-rheological experiments. HBE cultures, differentiated from primary cells at an air–liquid interface (ALI), are currently considered as reliable models of human airway tissues. We compare mucus collected from HBE cultures derived from healthy subjects, COPD patients and smokers free of COPD. As reported for other mucus in the literature, we found that HBE mucus flows as a shear-thinning elastic gel at the macroscale and as a low viscosity fluid with residual elastic properties at the microscale. Rheology-related, adhesive properties are another important feature of mucus transport, also playing a role in the trapping of foreign particles. Recently, the quantification of mucus adhesive properties has been addressed by performing experiments on bronchial epithelium cultures to quantify both cohesiveness and adhesion of mucus at the macroscale [23]. At the molecular scale, the binding of libraries of small molecules to mucin and other mucus components was recently quantified [24]. Here, optical tweezers were used to probe mucus mediated adhesion forces at the microscopic scale, showing that microstructures generate adhesion forces. Putting together these results on adhesion forces, mucus imaging and rheology measurements performed with mucus simulants at increasing concentration, we suggest a structure for HBE mucus that could reconcile the micro- and macro-flow responses.

2. Material and methods

2.1. Bronchial epithelial cultures at the air–liquid interface

Bronchial biopsies from six healthy patients, eight smokers free of COPD and five COPD patients were collected during fibreoptic bronchoscopy on a subsegmental bronchus of the left lower lobe at Arnaud de Villeneuve hospital (Montpellier, France). All donors signed a consent form after being informed about the biomedical research on airway epithelium performed thanks to their donation. The protocol was approved by the institutional ethics commission of Sud Méditerranée III (CHRU Montpellier—RECHMPL18_0222—NCT03187860). Primary human bronchial epithelial cells were obtained from bronchial biopsy specimens and cultured under ALI conditions [25], adapted from Gras *et al.* [26] and Gamez *et al.* [27]. Briefly, bronchial epithelial biopsies were mechanically dissociated and suspended in bronchial epithelial growth medium (BEGM, Lonza). After an expansion phase in monolayers, cells were plated on uncoated nucleopore membranes (24 mm diameter, 0.4 µm pore size, Transwell Clear, Costar) in a 1 : 1 mixture of BEGM and Dulbecco's modified Eagle's medium (DMEM, Lonza) until confluence. Then, the differentiation can take place after removing the medium above the cells. The culture medium is then provided only underneath the membranes. Cells were cultured for 28 days to obtain a polarized differentiated epithelial population with a mucociliary phenotype.

2.2. Mucus samples

Mucus, when efficiently released by the ALI cell culture, was gently collected with a micropipette every other day and stored at 4°C. Typically, for one ALI culture and after 2 days, 50–100 µl of secreted mucus was gathered. The day of collection was recorded for all our samples (D0 corresponding to the onset of differentiation conditions). The samples analysed in this study were gathered at D20 whenever possible, ranging in practice between D17 and D24.

2.3. Synthetic mucus samples

In order to obtain comparative models, several samples of polysaccharides solutions were prepared. We used the protocol described by Lafforgue *et al.* [28,29] using a galactomannan gum (Viscogum FA), and a scleroglucan (Actigum CS 6) from Cargill. First, the Viscogum was diluted in a 0.9 wt% NaCl solution at room temperature up to 0.5 wt% of the final solution and left to rest for 1 h. The Actigum was then progressively added up to a final concentration varying from 0.1 to 2 wt%. To favour cross-linking of the galactomannan chains, samples were stirred for 48 h before addition of a 0.02 M solution of Borax (disodium tetraborate) at a volume fraction of 2%. Samples were stirred for an additional hour before being used or stored at 4°C. The samples were used for the experiments no more than two weeks after preparation.

2.4. Macrorheology

Macrorheology experiments were performed using an Anton Paar MCR 502 and MCR 302 rheometer with a cone/plate geometry. The cone is 25 mm in diameter and has an angle of 1°, resulting in a gap of 218 µm at the cone edge. This geometry advantageously requires a small sample volume (80 µl). Experiments were performed at 20°C, using a low viscosity silicone oil deposited all around the sample edge to prevent evaporation. We carefully checked that experiments performed at 37°C and 20°C provided similar results. We also checked, by performing experiments with a humidity-saturated hood, that the presence

of silicone oil with a low viscosity of 20 mPa s did not induce an additional friction that could alter the rheological response. We waited 5 min between each test to relax residual stresses within the mucus. For dynamical rheological tests, each measurement was performed after three shearing cycles. In steady shear experiments, measurements were performed after a steady state was reached, in practice achieved in less than 30 s for the mucus. The choice of the cone/plate geometry is motivated by its small volume requirements (less than 80 µl) because of the small quantities of mucus at our disposal (less than 500 µl). Nevertheless, the use of this geometry with such a soft gel implies working close to the limit of sensitivity of the apparatus. To ensure the reliability of our measurements, we checked the different sources of errors such as the device torque limits or inertial effects, and computed the limits of validity [30], and found that our measurements fell within the confidence region (electronic supplementary material, figure SI1). We also used a strain imposed rheometer (ARES) to perform large-amplitude oscillatory shear (LAOS) macrorheology (see full details in electronic supplementary material).

2.5. Microrheology: sample preparation

Micrometre-sized beads were dispersed in mucus in order to be used as probes in active microrheology experiments. To this end, a small volume (approx. 0.5 µl) of an aqueous dispersion of beads was gently mixed with the collected mucus sample (approx. 50 µl). The final concentration of beads (0.004% v/v) was chosen in order to obtain microscopy chambers with area density lower than 400 beads per mm^2. Four different types of beads were used: silica beads (Bangs Laboratories Inc.), diameter of 1 µm or 4.5 µm; melamine resin beads (Fluka Analytical, Sigma-Aldrich), diameter of 5 µm; and carboxylated melamine resin beads, diameter of 3 µm. The mucus was then sandwiched between a glass slide and a coverslip (both PEGylated) separated by a mylar spacer. The thickness of the spacer (100 or 175 µm) and the dimensions of the chamber were chosen according to the available volume in order to minimize the residual air volume. After filling the chamber, the cell was rapidly (approx. 2 min) sealed with UV curable adhesive (ThorLabs NOA81) to prevent water evaporation. During UV exposure, the mucus was protected with a reflector (aluminium foil).

2.6. Microrheology: optical tweezers set-up

The optical tweezers set-up is mounted on an inverted optical microscope (LEICA DMI 3000 B) placed on an air-damped anti-vibration table (Workstation Series, Melles Griot). The optical trap is generated by the focalization of a laser beam (1064 nm laser YLM 5 W, from IPG Photonics) through a 100× (NA 1.4) oil immersion objective. The oscillating trap position is controlled via a pair of acousto-optic deflectors (AA optoelectronic). Alternatively, for lower frequencies and higher laser intensity, the sample is moved via a piezoelectric XY stage (Nano-Bio100 from MCL with a subnanometre accuracy). The trapped microsphere is imaged on a CCD camera (Basler Scout-F). A multifunction field programmable gate array (FPGA) is used to control the different devices and acquire data through a LabVIEW homemade program. The bead position is obtained by image correlation analysis under LabVIEW at a sub-pixel resolution (approx. 4 nm).

2.7. Microrheology: methodology

Microrheology experiments were performed by trapping a single bead using the optical trap and by applying a small sinusoidal displacement relative to the sample. The fluid viscoelastic properties, at the driving frequency ω, can be inferred from the bead position relative to the trap centre [31,32]. In the following, we consider a displacement of the stage $x_s^* = A_s e^{j\omega t}$ (with A_s the amplitude of the stage displacement) and a fixed trap. In the linear regime, a bead of radius a follows the sinusoidal displacement with a phase shift φ, and its trajectory is given by $x_b^* = A_b e^{j\omega t} e^{j\varphi}$ (with A_b the amplitude of the bead displacement). The strain is defined as $\gamma = (A_s - A_b)/2a$. Following the analysis by Shundo *et al.* [32] and other authors, the complex shear modulus $G^* = G' + j\,G''$ is related to the ratio of the fluid forces acting on the bead to its displacement with respect to the fluid (taking into account a $6\pi a$ factor for a spherical bead). The fluid forces being opposed by the restoring harmonic force of the trap of stiffness k_{OT}, one gets

$$G^* = \frac{k_{OT}\ x_b^*}{6\pi a(x_b^* - x_s^*)} = -\frac{k_{OT} A_b e^{j\varphi}}{6\pi a\ (A_b e^{j\varphi} - A_s)},$$

which leads to

$$G' = \frac{k_{OT}}{6\pi a}\ \frac{-A_b^2 + A_s\ A_b \cos\varphi}{A_b^2 + A_s^2 - 2\ A_b\ A_s \cos\varphi}$$

and

$$G'' = \frac{k_{OT}}{6\pi a}\ \frac{A_s\ A_b \sin\varphi}{A_b^2 + A_s^2 - 2\ A_b\ A_s \cos\varphi},$$

where G' and G'' are, respectively, the elastic and loss moduli of the surrounding fluid.

The stiffness k_{OT} of the trap can be obtained with two different methods [33]. The first method consists of recording the bead positions which result from thermal fluctuations of the bead within the trap. We infer the trap stiffness k_{OT} by fitting the distribution of the bead positions by a Boltzmann distribution $\sim \exp\{-E/k_B T\}$, with $E = k_{OT}\ x_b^2/2$ and $k_B T$ the thermal energy. This method was used for all mucus collected from ALI cultures. The measured laser power P at the entrance of the microscope objective ranged from 20 to 100 mW. For adhesion force measurements and for the most elastic samples of synthetic mucus (greater than 0.5 wt% in Actigum), a higher laser intensity ($P > 1$ W) was required in order to keep the bead trapped during the motion. In this configuration, the Brownian motion could not be detected. We then calibrated the trap stiffness in water as a function of the laser power using the drag force method [33], exploiting the fact that the optical index of the samples ($n \approx 1.335$) is very close to the index of water. We checked that both calibration curves overlapped according to a linear dependence $k_{OT}(P)$ for a given type of beads. In our experiments, we imposed $A_s = 1$ µm or $A_s = 0.5$ µm depending on the elasticity of the sample. We measured both A_b and φ for a range of frequency f between 0.09 and 50 Hz. All experiments were conducted at room temperature. Nevertheless, we measured the temperature of the sample near the trap which could reach 30°C, because of local heating generated by the bright light illumination and by the laser at high power. In a previous work [34], we showed that a temperature increase does not significantly affect the mucus rheological behaviour on logarithmic scales. The set-up and the protocols were first validated with a well-studied viscoelastic model system of giant micelles for which we obtained rheological curves very close to the macrorheological ones [35,36].

2.8. Optical tweezers: adhesion forces

Two approaches were used to assess mucus local adhesion forces and study their properties.

In a first set of experiments, we manipulated isolated beads (melamine resin, diameter 5 µm) that previously rested on the PEGylated coverslip. Once a bead reached the bottom of the chamber by sedimentation, it was left in contact with the glass coverslip for a minimum of 10 min before trapping it with the

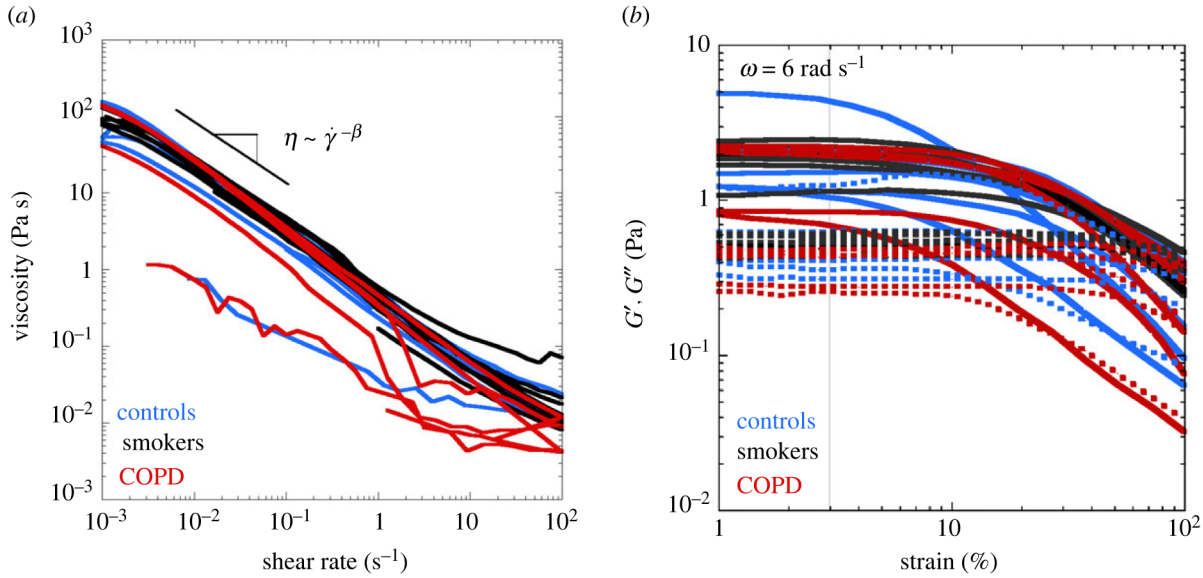

Figure 1. (*a*) Mucus flow curves obtained from macrorheology measurements. Viscosity as a function of shear rate for mucus collected from human bronchial mucus corresponding to healthy controls ($N = 6$, blue), smokers ($N = 8$, black) and patients with COPD ($N = 5$, red). (*b*) Strain sweep experiments. Storage G' and loss G'' moduli as a function of the strain (solid and dotted lines respectively) at $\omega = 6$ rad s^{-1}. Onset of the nonlinear regime was set at 2.7% (grey vertical line).

optical tweezers. Detaching the bead from the surface then required a high laser power (approx. 1 W), much larger than the power necessary to oppose the weight of the bead or to detach one in a chamber filled with pure water. The bead was then lifted about 10–20 µm away from the glass coverslip before applying a periodic back and forth displacement $X(t)$ relative to the trap centre (around the bead position), parallel to the coverslip plane, with an amplitude of 10 µm and at a constant velocity $v = 0.88$ µm s^{-1}. We then computed the force F_{xy} acting on the bead from the bead displacement X_{bead} from the trap centre using the previously calibrated trap stiffness k_{OT}: $F_{xy} = k_{OT}\, X_{bead}$.

In the second approach, performed at much lower laser power (10–30 mW), we focused on the initial detachment of a bead from a solid surface. To this end, a set of pillars were fabricated on a coverslip by replica moulding. A PDMS mould was first prepared by microlithography. A drop of UV curable adhesive (ThorLabs NOA81) was then sandwiched between a coverslip and the mould, before being cured. The mould was then gently peeled off and the coverslip used to create a chamber as previously explained. Using optical tweezers, we drove a 4.5 µm diameter silica bead near the vertical wall of a pillar. Once trapped, the bead was initially kept in contact with the NOA81 wall for at least one minute before being pulled away very slowly (less than 0.1 µm s^{-1}), up to a fixed distance of 10 µm. The evolution of the resulting adhesion forces, $F_{xy} = k_{OT}\, X_{bead}$, was then monitored by recording the bead position from the trap centre at 30 frames per second for 2 min or until rupture of the adhesion.

2.9. Cryo-scanning electron microscopy

To image the mucus network, we analysed six mucus samples collected from cell cultures from two healthy controls, two smokers and two patients with COPD. Mucus samples were inserted between two high-pressure freezing (HPF) specimen carriers dedicated to cryofracture (Leica) and were loaded immediately into a HPM100 HPF machine (Leica). Samples were subsequently fixed and frozen within 5 ms at 2050 bar before being transferred into cryovials in liquid nitrogen. Then the HPF specimen carrier with frozen mucus was inserted into the preparation chamber (Quorum PP3000T). For insertion, specimen shuttle cryo stubs and HPF specimen carrier adapter were used following the protocol from Payre *et al.* [37]. After a fast transfer under vacuum in the preparation chamber, the samples were fractured at −140°C, sublimed at −95°C during 30 min and then coated by platinum sputtering. They were finally transferred in the cryo-SEM Quanta 250 FEG chamber and kept at −140°C during observation with a FEI Quanta 250 FEG scanning electron microscope at an accelerating voltage of 5 kV.

3. Results and discussion

3.1. Macrorheology

Shear rheology experiments were performed with a controlled-stress rheometer mounted with a cone/plate geometry, at room temperature. Both steady and dynamic experimental conditions were explored.

3.1.1. Shear flow and yield stress

The shear flow response of mucus samples was measured by imposing a steady shear with increasing shear rates. Figure 1*a* represents the shear viscosity η versus shear rate $\dot{\gamma}$ measured on mucus collected from ALI cultures of included patients according to their group. No significant difference was observed. The between-group variability in amplitude was deemed comparable to the between-sample variability recorded within the same group.

The steady shear viscosity strongly decreases through the entire range of explored shear rates for all assessed samples irrespective of the group. This strong shear thinning behaviour can be described by a power law $\eta \propto \dot{\gamma}^{\beta}$ with an averaged exponent $\beta \approx -0.85$. For the smallest shear rate experimentally accessible, $\dot{\gamma} \sim 10^{-3}$ s^{-1}, a viscosity $\eta \approx$ 100 Pa s was found but no plateau was recovered. When representing the flow curve as shear stress versus shear rate (electronic supplementary material, figure SI2A), a yield stress could be evidenced. At very low shear rates (approx. 10^{-3} s^{-1}) the measured stress does not tend to zero but to a yield stress value, $\tau \approx 0.05$–0.2 Pa. The same range is obtained for the stress value at the end of the linear plateau on the same plot. In addition, creep tests also showed that mucus flows only above a yield stress (0.05 Pa) of the same order

of magnitude (electronic supplementary material, figure SI2B). Yield-stress fluids display a solid-like behaviour at low stress and flow only above a critical applied stress, after the solid structure collapses. Such yield-stress properties were shown to play a role in snail locomotion in the case of pedal mucus [12]. The difficulty to precisely and unambiguously determine the yield stress, depending on the detailed experimental protocol or the measurement geometry, has been well documented in the literature recently [38–40]. Here, we show that mucus collected from HBE cultures are soft yield-stress fluids with a yield stress ($\tau \approx 0.05$–0.2 Pa) very small if compared with the typical range of values reported in the literature for other materials such as emulsions, foams, colloidal suspensions or granular media. In the airways, flowing only above a yield stress could be advantageous, favouring trapping of foreign particles at low stress and flow above a yield stress reached when coughing for instance. Indeed, the shear stress due to air flow can vary in a range from 1 to 10^4 Pa, depending on the bronchial level, from air flow due to breathing up to the shear generated during coughing [23]. On the reverse, a rough estimate of the shear stress generated by a swimming pathogen with velocities in the range 1–100 µm s^{-1} gives values from 10^{-4} up to 10^{-2} Pa, lower than the yield stress we measured for mucus.

3.1.2. Dynamic shear response

Dynamic shear experiments were performed to assess mucus linear viscoelastic properties. An oscillatory stress was applied to the sample at a frequency ω. We first determined the range of amplitudes for which the fluid response is linear. In figure 1*b*, the elastic G' and loss G'' moduli measured for $\omega = 6$ rad s^{-1} are reported for increasing strain amplitudes. We found for most curves that both moduli are constant for strains lower than 10%. Nevertheless, because in some rare cases a decrease for lower strain amplitudes was obtained, we set the limit of the linear response at 2.7%. This limit is also valid for the highest frequency used in our experiments.

LAOS analysis allows one to explore the nonlinear behaviour of complex fluids. Cough for instance can generate large shear stresses, motivating the use of LAOS to characterize mucus rheology in this regime. We thus performed a LAOS flow protocol on two samples with a strain-imposed rheometer and over a 10–1000% strain amplitude range (electronic supplementary material, figure S3 and table S1). For both samples, increases in the nonlinear coefficients e_3/G'_1 and S were obtained. We found that S, which should be null in the linear regime, was always greater than 0, ranging from 0.3 up to 0.64. In addition, S positive sign reveals a strain stiffening behaviour at high shear strains. These results are comparable to those obtained for gastropod pedal mucus [12,41], or for mucus collected from horse lungs [7,11] or mucus simulants [42]. By contrast, onset of a nonlinear response in the presently studied HBE-released mucus was recorded for much smaller deformations. Further experiments should be addressed to determine whether this approach has a relevant diagnostic value.

Within this linear viscoelastic regime, the fluid response is mostly elastic, with a storage modulus (G') nearly twice as large as the loss modulus (G''). A significant decrease in G' is observed for strain larger than 10%, whereas G'' remains almost constant up to 50%. For strain amplitudes above 50%, the elastic and dissipative contributions are comparable in magnitude. We also checked whether the linear shear response was correlated with the day of mucus collection by measuring G' and G'' of mucus from the same well from Day 10 to Day 30 (electronic supplementary material, figure SI4) and found that the measured shear rheology is independent of the culture level of maturity.

In figure 2*a*, we show the linear viscoelastic moduli, G' and G'', obtained by performing a frequency sweep at a strain of 1%, within the linear regime. In the range of experimentally accessible frequencies ($0.6 < \omega < 60$ rad s^{-1}), the elastic contribution (G') dominates over the dissipative one (G''). The elastic modulus increases with the applied frequency according to a power law, with an exponent $\alpha \approx 0.2$, close to 0 as expected for an elastic gel (figure 4). Shear-thinning and such an elastic behaviour at the mascropic scale are in agreement with previous literature dedicated to mucus rheology as reviewed in [18] for various mucus and methods.

In both figures 1*b* and 2*a*, curves obtained for control, smokers and COPD mucus are plotted in different colours. No significant difference was observed between sets of curves corresponding to different patients groups as further illustrated in figure 4, which compares the moduli amplitudes set as values of G' and G'' measured at 6.3 rad s^{-1} (1 Hz) and the power-law exponents α. The large variation within a group is comparable to variation between groups.

3.2. Microrheology

To probe the mucus flow behaviour at a length scale comparable to the cilia size, an optical tweezer experiment was set up and a microscopy chamber was prepared by mixing beads with the mucus. A few aggregates made of immobilized beads strongly embedded in organic material are observed within the mucus. However, most beads are isolated and slowly sediment towards the coverslip. Brownian motion can be easily observed and indicates a rather weak elasticity. Microrheology experiments have been performed on such beads before their sedimentation on the coverslip or after they have been detached from it. In a typical experiment an oscillatory displacement was applied to a trapped bead with local strains in the range 5–20% and the resulting force acting on the bead was measured. Experiments using beads of different surface chemistries (carboxylated melamine resin and silica), and of different diameters ranging from 1 to 5 µm, showed no significant differences in the viscoelastic response (electronic supplementary material, figure SI5). In the following, we describe results obtained for melamine resin beads of 3 µm in diameter.

The transition from a linear to a nonlinear regime was evaluated by performing a shear strain sweep at $\omega = 6$ rad s^{-1} (electronic supplementary material, figure SI6). The onset of nonlinearity appeared between 10 and 20% in strain amplitude. All experiments were thus performed at strain values lower than 20%. The G'' values reported in figure 2*b* were obtained by averaging 2–18 measurements performed on different beads and at different spatial locations within the sample. Mucus being a material heterogeneous at various length scales, it is important to specify that we think that the mucus we collected on HBE cultures was mainly homogeneous at a macroscopic scale: it was transparent and did not exhibit macroscopic regions of different structure. When we displaced the probe with the optical tweezer in different

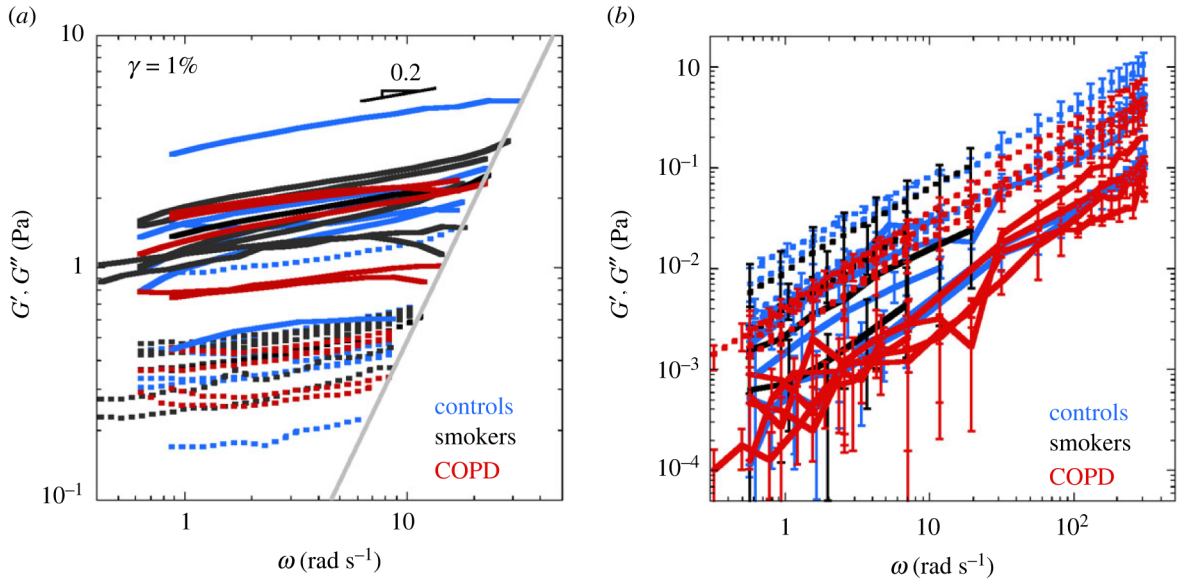

Figure 2. (*a*) Mucus viscoelasticity measured in macrorheology tests: storage G' (solid line) and loss G'' (dotted line) moduli as a function of the frequency measured in the linear viscoelastic regime ($\gamma = 1\%$). The slope corresponding to an exponent value of 0.2 is represented as a comparison. The grey line indicates the instrumental limits. Mucus samples are collected from human bronchial epithelial cultures derived from biopsies of healthy controls ($N = 6$, blue), smokers ($N = 7$, black) and patients with COPD ($N = 5$, red). (*b*) Mucus viscoelasticity measured in microrheology, using optical tweezers. Storage G' (solid line) and loss G'' (dotted line) moduli as a function of the frequency, with a displacement amplitude of 1 µm measured on mucus collected from HBE corresponding to five healthy patients (controls in blue), two smokers (black) and five patients with COPD (red). The curves represent the mean value of N measurements performed in several spatial locations within the preparation chamber. The error bars represent the mucus heterogeneity with the minimum-to-maximum values obtained from these N measurements.

areas of the sample, we measured consistently the same rheological response. In some rare cases nevertheless, the bead was sticking to structures invisible under the microscope but that were detectable because of the restoring forces generated when moving the probe with the optical tweezer. We also observe some aggregation of the introduced probes within 24 h indicative of the presence of sticky structures in the sample. The results shown correspond to mucus samples derived from ALI cultures of healthy patients (controls, $N = 5$), smokers ($N = 2$) and patients with COPD ($N = 5$). The elastic moduli were at least two orders of magnitude smaller than those obtained from macrorheology experiments on the same samples as illustrated in figure 3. Besides, contrarily to the elastic response obtained with macrorheology, the rheological response measured at a local microscopic scale was dominated by dissipation: (i) the loss modulus was larger than the elastic modulus by a factor ≈ 5 (figure 2*b*) over the entire range of explored frequencies ($0.6 < \omega < 300$ rad s^{-1}); (ii) G'' increases almost linearly with ω, with a scaling law exponent α in the range 0.75–1, α being expected equal to 1 for a Newtonian fluid. Similar results were obtained using the passive microrheology methods based on the Brownian motion in agreement with the literature [43–45]. The storage G' and loss G'' moduli measured at 6.3 rad s^{-1} (1 Hz) extracted from the macrorheology and microrheology are compared in figure 4. G' and G'' values span more than one order of magnitude. Micro- and macro-moduli differ by at least two decades. The reported power law exponents α highly differ between micro- and macrorheology experiments, reflecting the dissipative ($\alpha \approx 0.75$–1) versus the elastic ($\alpha \approx 0.05$–0.25) behaviour of these mucus samples (figure 4*b*). No significant difference was recorded between the three different groups for G' and G'', whereas small but significant ($p < 0.05$) differences in power law exponent were reported. In table 1, p-values referring to bilateral T-tests are reported showing differences

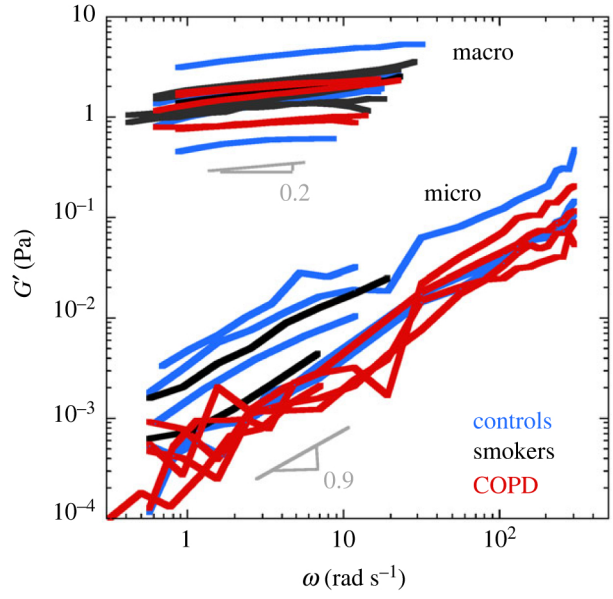

Figure 3. Direct comparison of the elastic modulus G' measured as a function of the frequency in macrorheology (macro) using a standard rheometer and in microrheology (micro) using an optical tweezer, for the three groups controls (blue), smokers (black) and COPD patients (red).

between controls and COPD samples for microrheology experiments and between smokers and COPD samples for macrorheology experiments. These results suggest that mucus secreted by ALI epithelial cultures from COPD patients were slightly more fluid-like at a microscale and slightly more elastic at a macroscopic scale as compared to mucus from healthy patients. These differences remain small and would benefit from larger values of N since we obtained large variation within groups that made differences between groups difficult to evidence.

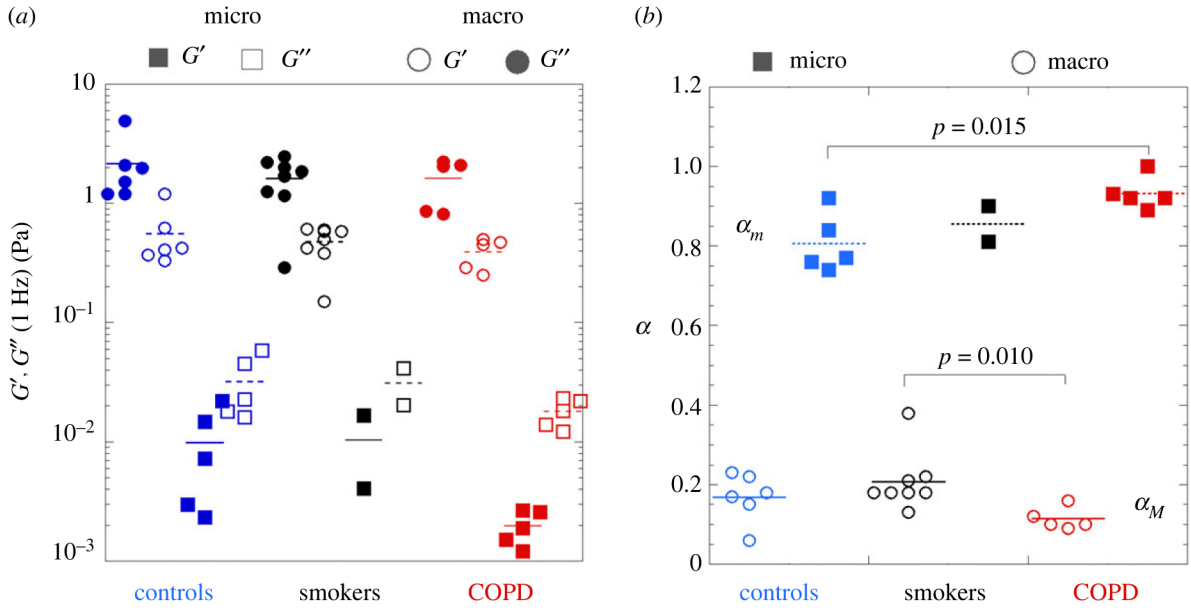

Figure 4. Comparison between macrorheology (circles) and microrheology (squares) experimental results obtained for collected mucus samples. Mucus was collected from HBE cultures corresponding to: controls (blue), smokers (black) and COPD (red). (*a*) The storage G' (filled symbols) and loss G'' (open symbols) moduli measured in the linear regime at 1 Hz, in macrorheology (data from figure 2*a*) and in microrheology (data from figure 2*b*). The lines represent the mean value. The *p*-values (table 1) are obtained with a bilateral *T*-test and reported on the graphs only when significant ($p \leq 0.05$). (*b*) The exponents α_M of the power law of $G'(\omega)$ measured at the macroscale (circles) (data from figure 2*a*) and α_m of $G''(\omega)$ measured at the microscale (squares) (data from figure 2*b*).

Table 1. *p*-values for: controls/smokers, controls/COPD and smokers/COPD. Several rheological parameters are presented. In macrorheology data: the values of the storage G' and loss G'' moduli in linear regime at 1 Hz (reported in figure 4*a*), along with the G'/G'' ratio at 1 Hz and also the stress value within the nonlinear regime for which $G' = G''$ (see data figure1*b*); the exponent α_M of the power law fit of $G'(\omega)$ (reported in figure 4*b*). In microrheology: the values of the storage G' and loss G'' moduli at 1 Hz (reported in figure 4*b*), along with the ratio G'/G'' at 1 Hz, and the exponent α_m of the power law fit of $G''(\omega)$ (reported in figure 4*b*). *p* was computed for *N* experiments per group with a bilateral *T*-test and reported when $N \geq 5$ only. Significant values are in italics ($p \leq 0.05$).

	macrorheology					microrheology			
p-values	G' (1 Hz)	G'' (1 Hz)	G'/G''	stress at $G' = G''$	α_M	G' (1 Hz)	G'' (1 Hz)	G'/G''	α_m
controls/smokers	0.417	0.597	0.164	0.404	0.302	—	—	—	—
controls/COPD	0.435	0.289	0.788	0.678	0.091	0.104	0.168	*0.027*	*0.015*
smokers/COPD	0.998	0.282	0.139	0.265	*0.010*	—	—	—	—

For the same samples, relevant biochemical or biophysical mucus properties were assessed (pH, dry mass, salt and protein content as shown in table 2) and did not show any significant difference between the groups: none of the *p*-values were found to be greater than 0.05 (table 2). No correlation between the dry mass or the protein concentration and rheology parameters was found (electronic supplementary material, figure SI8). Nevertheless, the specific assessment of MUC5B and MUC5AC could be worthwhile, but has to be investigated with care as recently highlighted methodological issues indicated a heterogeneous distribution of these key proteins [21]. We thus consider, given the poor accessibility to HBE mucus and the dispersion in the rheological measurements, that HBE linear rheology performed either at the microscopic or macroscopic length scale is not the proper marker for COPD or severe asthma diagnosis. It remains yet to be evaluated whether nonlinear rheology (LAOS) could be a more sensitive physical parameter to be used as diagnosis marker.

3.3. Comparison with mucus simulants

The discrepancy between micro- and macrorheology previously reported for other mucus types [7,13,19] and presently confirmed on collected HBE mucus remains to be further investigated. To this purpose, we performed micro- and macrorheology assays on mucus simulants in order to compare the two rheology responses on gels of increasing concentration. The question we address here is about the relationship between the micro/macro mismatch and the mucus concentration and structure. These mucus simulants, made of polysaccharides, were shown by others to exhibit macrorheology responses that fit with the *ex vivo* mucus rheology [28,29,42]. Contrarily to native mucus or

Table 2. Between-group comparisons for mucus biochemical and biophysical properties (controls, smokers and COPD). The values are the mean ± standard deviation of all subjects in each group. Differences between groups were found statistically insignificant ($p \leq 0.05$). The *p*-values are indicated in the three last rows.

	pH	dry mass (%)	proteins (g l^{-1})	Na^+ (g l^{-1})	Cl^- (g l^{-1})	HCO_3^- (g l^{-1})
controls	8.0 ± 0.8 ($N = 10$)	1.96 ± 0.34 ($N = 10$)	1.37 ± 0.39 ($N = 4$)	3.63 ± 0.06 ($N = 3$)	3.56 ± 0.29 ($N = 3$)	0.99 ± 0.60 ($N = 3$)
smokers	7.8 ± 0.6 ($N = 8$)	1.85 ± 0.41 ($N = 9$)	1.49 ± 0.34 ($N = 6$)	3.64 ± 0.23 ($N = 5$)	3.92 ± 0.42 ($N = 5$)	0.41 ± 0.28 ($N = 4$)
COPD	8.1 ± 0.4 ($N = 5$)	1.82 ± 0.55 ($N = 5$)	1.39 ± 0.69 ($N = 4$)	3.62 ± 0.02 ($N = 4$)	3.66 ± 0.18 ($N = 4$)	0.91 ± 0.51 ($N = 3$)
p(controls/ smokers)	0.58	0.5	0.61	0.92	0.2	
p(controls/COPD)	0.85	0.55	0.95	0.84	0.61	
p(COPD/smokers)	0.4	0.92	0.8	0.85	0.26	

mucus collected on HBE, mucus simulant composition can be tuned. We measured the micro- and macrorheology properties of mucus simulants of various compositions, respectively in the range 0.1–1 wt% and 0.1–2 wt% (figure 5). Concentrations above 1% could not be accessed using optical tweezers because moduli were too high and the frequency range explored is also smaller (0.5–7 rad s^{-1}) than for the standard rheometer (5–60 rad s^{-1}) except at the lowest concentration (0.1%).

The elastic and loss moduli both increase with the frequency according to a power law. The power law exponent α measured for G' can be used as a marker of the elastic to viscous balance: α tends to 0 for purely elastic materials and to 1 for purely viscous fluids. At both macroscopic and microscopic length scales, G' and G' increased with the concentration as the exponent α decreased, meaning that elasticity increased with the concentration in polysaccharides. At 1%, G' measured at 1 rad s^{-1} for micro- and macrorheology were comparable: respectively, 50 and 25 Pa, G' being larger than G', whereas the exponent α was two times smaller at the macroscale. At low concentration, around 0.1% which is closer to HBE collected mucus (figure 5*c*), the gap between macro- and micro-moduli increased: the complex fluid behaved as a viscous fluid at the microscale and as an elastic fluid at the macroscale. In figure 5*c*, the exponents α obtained for both measurements were compared. For the lowest concentrations, micro- and macro-exponents had different values. The macro-exponent was lower indicating a more elastic behaviour than at the microscale. Nevertheless, both exponents decreased with the concentration, with a higher rate for micro than for macro, and converged towards the same values at high concentration. This suggests that the discrepancies in the mechanical responses measured at different length scales are mainly observable at low concentration when the network mesh size is large, and become negligible when the polymeric network reaches a volume fraction, i.e. when the sample and the structures formed by the mucus simulant become denser and less heterogeneous. Using cryo-SEM, natural mucus networks and mucus simulant structures were consistently reported as being multi-scale heterogeneous networks [5–7,21,28,29,42,46]. We performed cryo-electron microscopy on HBE collected mucus, at different magnifications as shown in figure 5*d–f*. Mucus structure was found to be highly heterogeneous, filamentous at the largest length scale (figure 5*e*), and more foam-like structured at smaller scales (figure 5*d,f*). These electron microscopy data are to be taken with caution. They probably reflect the denser regions of the gel and it is also plausible that the fixing/freezing processes might have concentrated the mucus in some parts of the sample. The native hydrated structure of the mucus was recently reported by Meziu *et al*. [21], by combining confocal and STED methods and suggests that porous structures observed with cryo-electron microscopy result from the fixing protocol. The revealed mucus structure obtained with high-resolution immunostaining [21] is found to be continuous: mucins are present in all the mucus sample without discontinuity reported from electron microscopy but nevertheless with a heterogeneous protein composition. This composition heterogeneity is certainly a key ingredient not only for drug and particle transport in mucus but also to explain the length scale dependent flow response reported.

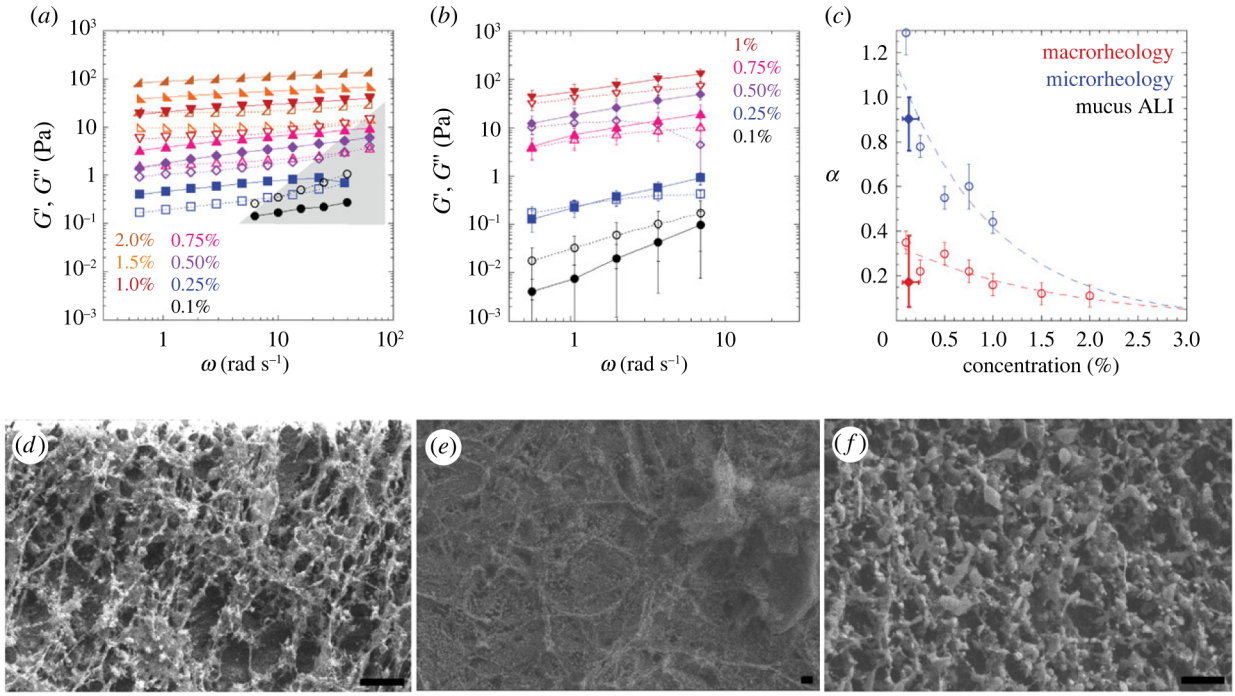

Figure 5. (*a–c*) Comparison of macro- and microrheology results on a synthetic mucus at several concentrations. Storage G' (filled symbols and solid lines) and loss G'' (open symbols and dotted lines) moduli as a function of the frequency measured at seven different concentrations of Actigum: 2 (dark orange right triangles), 1.5 (orange left triangles), 1 (red triangles down), 0.75 (pink triangles up), 0.5 (violet diamonds), 0.25 (blue squares) and 0.1% w/w (black circles), performed in macrorheology (*a*) and in microrheology (*b*). In (*a*), the grey triangle indicates the data beyond the instrumental limitations. (*c*) Power law exponent α of $G'(\omega)$ as a function of the Actigum concentration of polysaccharide solution (open circles) measured from macrorheology (red) and microrheology (blue). Error bars represent the power law fit error and the dashed lines are guides for the eye. The filled diamond symbols are the corresponding averaged α values extracted from figure 4 and plotted as a function of the averaged concentration in proteins (table 2). (*d–f*) Cryo-SEM representative images of mucus collected from HBE ALI cultures. Illustration of the heterogeneous structures obtained at different length scales. (*d,e*) From a healthy control subject derived mucus sample and (*f*) mucus from a COPD patient. Scale bar: 1 µm.

3.4. Adhesion properties at the microscale

Microrheology experiments were performed using probes that were at a distance from the glass slides larger than 20 µm. Nevertheless, when trapping a bead closer to the glass slides (less than or equal to 10 µm), we obtained much larger forces (greater than or equal to 2 pN) resisting the bead motion. Converting the forces measured for a given displacement into a rheological response resulted in an elastically dominated response of the mucus (electronic supplementary material, figure SI7), instead of a dissipative-dominated behaviour. The typical values obtained for the elastic modulus are at least one order of magnitude larger than those measured in the bulk. Mucus thus appeared more elastic in the neighbourhood of a solid substrate. Similar forces also appeared when two beads, after contact for several minutes, were pulled apart from each other. We thus developed a protocol to measure these forces and investigate their origin.

The experiment is illustrated in figure 6*a*, where the relative displacement of a bead with respect to the chamber at a constant velocity of 0.88 µm s^{-1} and the resulting force acting on the probe are both given as a function of time. The bead was almost free to move in the range [−5 µm, 8 µm] (region 1) but experienced an effective restoring force outside this region that increased when the probe was pulled away (region 2 for $x < -5$ µm) and decreased when going back (region 3). A similar restoring force is observed in the other direction, when $x > 8$ µm. During the remaining parts of the cycle, the force acting on the bead was much lower, corresponding to the viscous drag with some fluctuations due to thermal noise. A sketch illustrating our interpretation is provided in figure 6*a*: when the bead is in contact with the surface, at rest, adhesive structures that could be similar to the filaments we observed by electron microscopy (figure 5*d–f*) adhere both to the bead and to the glass surface, thereby connecting them. Such structures could form spontaneously by diffusion and adhesion of the glycoproteins on both substrates, bridging them when they are close enough, or because mucus was mechanically squeezed between the bead and the substrate as occurs for tack polymers [47]. When the bead is pulled away via the tweezers, these loose adhesive structures made of mucus are initially unfolded (region 1 schemed in figure 6*a*) up to a deformation above which they are continuously stretched (region 2) until full extension, corresponding to the maximal displacement of the bead and to forces in the range 20–300 pN. When the bead is pulled back, the extensional force decreases down to zero (region 3). At this stage, the filament is loose again. We performed five similar experiments over several cycles. In some cases, we observed that this maximal force increased with the number of cycles indicating an evolution of the adhesive structure cohesiveness and/or adhesion to the surfaces, whereas in other experiments it remained constant.

In the second experiment (figure 6*b*), still using optical tweezers, we studied more accurately the first steps of adhesion and detachment. The bead was put in contact with a vertical interface for approximately one minute, then it was slowly pulled away (less than 0.1 µm s^{-1}), at a distance

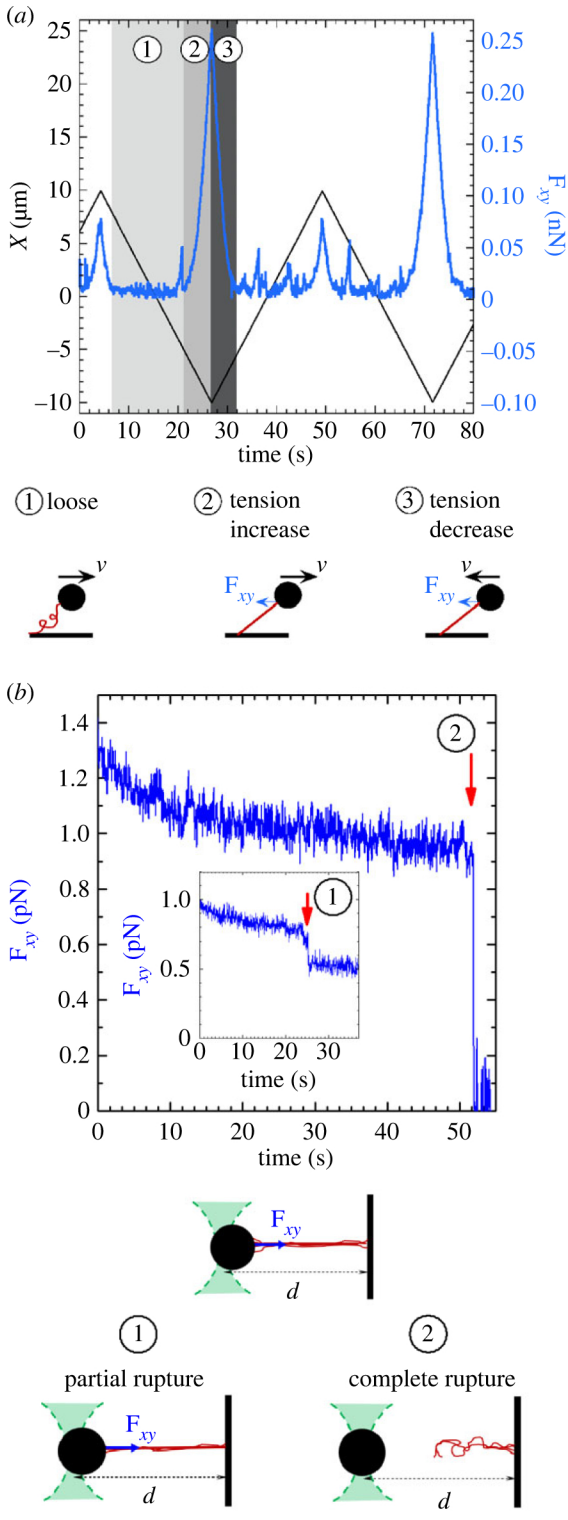

Figure 6. Mucus adhesion forces. Forces are measured with optical tweezers, by trapping 5 µm melamine beads. (*a*) Force response under oscillatory pulling at a constant speed $v = 0.88$ µm s^{-1} on a 10 µm amplitude, represented by the triangular displacement $X(t)$ of the mucus relative to the trap centre (black line). The force exerted on the trapped bead (blue line) is computed from the bead displacement $\mathbf{X_{bead}}$ using the calibrated trap stiffness k_{OT}. The drawing illustrates the hypothesis that mucus filaments may be responsible for the tension forces measured, when pulling on a bead after it has been put in contact with the glass slide. At small displacement (1) filaments are loose and no force is measured; at higher displacement the filaments exert a restoring force F_{xy} (2) which is released as soon as the displacement is decreases (3). (*b*) Force versus time in response to an imposed displacement. The inset corresponds to an experiment performed for another experimental run. After 1 min of contact with a wall, a 4.5 µm diameter silica bead is held at a constant distance *d* from the wall. Example of partial (1) and complete (2) release of the tension exerted on the bead, which might be potentially caused by the rupture of elastic mucus filaments.

ranging from 5 to 20 µm. A restoring force (much weaker than in the previous case) was measured, indicative of a structure tethering the bead to the vertical wall formed when the bead was in contact with the vertical interface. We then stopped the displacement, maintained the bead at a fixed position and measured the restoring force time variation. This experiment provided an insight on the time scales and mechanisms associated with the relaxation of this adhesion force. In particular, as exemplified in figure 6*b*, we observed a relaxation of this force over tens of seconds punctuated by sudden force drops that might correspond either to partial rupture or complete rupture of the adhesive structures or of their adhesion to the surfaces. These preliminary experiments indicate that adhesive structures, potentially filamentous as suggested by our cryo-SEM observations, are formed by the mucus constituents. These structures could bridge objects, leading to bead aggregates as we observed in our microscopy chamber or to cell aggregates [34]. Optical tweezers could be a technique of interest to examine how they form and how their dynamics under stretch connects with the viscoelastic properties of the mucus and also with the role of dissipation, measured using peeling experiments on HBE cultures [23] as well as at a molecular scale [48].

Taken together, all of these results led us to propose a structural picture of the mucus, not far from previously proposed representations as two-network or foam-like models [7,13]. Recent data on mucus, imaging of several mucins spatial distribution [21], self-assembly molecular dynamics (MD) simulations [22] and the rheological and adhesive behaviour reported here, indeed led us to hypothesize that mucus heterogeneous structure could be composed of filamentous adhesive structures, rich in GFMs, forming a large mesh-size network within a very soft gel poorly concentrated in GFMs, which would be the mucus fraction mainly probed in microrheology (figure 7). In this description, the GFM-rich network represents a low fraction of the mucus sample and is loose, i.e. its mesh size is large compared to our probe and to the filament persistence length. We expect then that in a cone/plate rheometer, elastic filaments connecting the bottom and the top of the rheological chamber result in an elastic gel response, whereas a microparticle, small compared with the filament network mesh size, essentially probes the very soft gel (figure 7*a*). Indeed, in the structure we propose, the microparticle will rarely encounter an elastic filament and will essentially probe a soft gel. The fact that adhesive structures form close to substrates suggests that these structures are resulting from a remodelling of the network due to the stickiness of the filaments or to an attractive interaction of mucins with substrates. We previously showed how the presence of a substrate (cells or tissues) plays a role in the elastic behaviour of the mucus [34], and thus potentially in the spatial distribution or recruitment of mucins. At higher mucus concentration, the protein concentration could increase in both the filamentous network and in the soft gel, and more importantly, the partition between the two could change, leading to a denser network of filaments (figure 7*b*), that could explain the convergence of the two rheological responses at higher concentrations, obtained with the mucus simulants and also reported for concentrated HBE mucus [43]. More experiments would be required to validate this picture of the mucus structure, using the Meziu *et al*. protocol for instance [21] to infer MUC5B spatial distribution or MD simulations [22] to understand further the structures formed by mucins at various scales.

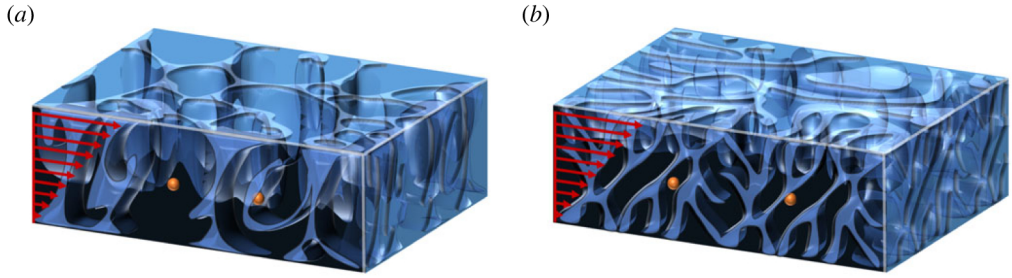

Figure 7. The structural picture of the gel we propose is a loose network of filamentous elastic sticky structures, rich in GFMs, filled with a very soft gel diluted in GFMs, resulting in an almost Newtonian flowing behaviour. As the concentration in mucins increases (*a* to *b*), the fraction of filamentous structures increases and makes the elastic network denser. In a cone/plate rheometer, we could consider that this loose network of elastic filaments connecting the bottom and the top of the rheological chamber results in an elastic gel response, whereas with a microscopic probe the particle essentially probes the soft gel.

4. Conclusion

Combining micro- and macrorheology, we characterized the rheological response of mucus collected from bronchial epithelial ALI cultures. An elastic, shear-thinning and yield-stress behaviour is the hallmark of the HBE mucus at a macroscopic scale, whereas at a microscale dissipation is predominant. Highly heterogeneous elastic structures are however present generating heterogeneous adhesion forces acting on probe particles near surfaces. We here reported original adhesion experiments performed at the scale of a cilium that further support a mucus structure made of a loose network of sticky elastic filaments embedded in very soft gel. The structure we propose, likely explains the apparent discrepancies observed between micro- and macrorheology responses when dealing with small concentration in mucus as is the case for HBE collected mucus. Based on these new experiments, novel approaches should be designed for further investigation on the origin and regulation of adhesion properties of the airway mucus and also on the imaging of the mucin network using STED and labelling specific proteins to characterize their spatial distribution and understand further the structure of HBE mucus.

Ethics. The protocol was approved by the institutional ethics commission of Sud Méditerranée III (CHRU Montpellier—RECHMPL18_0222—NCT03187860). Patients provided written consent.

The data are provided in the electronic supplementary material [50].

Authors' contributions. M.J.: data curation, investigation, methodology, validation, writing—review and editing; D.D.: data curation, formal analysis; C.B.: data curation, investigation, methodology, supervision, writing—review and editing; K.B.: data curation; A.F.: methodology; I.V.: funding acquisition, writing—review and editing; L.C.: methodology, supervision, writing—review and editing; A.B.: funding acquisition, project administration, supervision, writing—review and editing; G.M.: conceptualization, funding acquisition, investigation, project administration, supervision, writing—original draft, writing—review and editing.

All authors gave final approval for publication and agreed to be held accountable for the work performed therein.

Conflict of interest declaration. We declare we have no competing interests.

Funding. This work has been supported by: Labex Numev (ANR), Fonds de dotation 'Recherche en Santé Respiratoire' FSFR AAP2015-2-053, Vaincre la Mucoviscidose AP2016 RF20160501673, ANR Mucocil 13-BSV5-0015, CHU Montpellier (AOI RECHMPL18_0222 NCT03187860) and Medicine Biology Mediterranée.

Acknowledgements. We thank Payre Bruno of CMEAB (centre de microscopie électronique appliquée à la biologie de l'université Paul Sabatier de Toulouse III) for scanning electron microscopy observations, Gontier Etienne of BIC (Bordeaux Imaging Center) for high-pressure freezing, and Véronique Chamel (CEA Grenoble, France) for protein quantification. We thank G. H. McKinley for providing us the MITLAOS Matlab code.

References

1. Kirkham S, Sheehan JK, Knight D, Richardson PS, Thornton DJ. 2002 Heterogeneity of airways mucus: variations in the amounts and glycoforms of the major oligomeric mucins MUC5AC and MUC5B. *Biochem. J.* **361**, 537–546. (doi:10.1042/0264-6021:3610537)
2. Kesimer M *et al.* 2018 Airway mucin concentration as a marker of chronic bronchitis. *New Engl. J. Med.* **377**, 911–922. (doi:10.1056/NEJMoa1701632)
3. Hogg JC *et al.* 2004 The nature of small-airway obstruction in chronic obstructive pulmonary disease. *New Engl. J. Med.* **350**, 2645–2653. (doi:10.1056/NEJMoa032158)
4. Demouveaux B, Gouyer V, Gottrand F, Narita T, Desseyn JL. 2018 Gel-forming mucin interactome drives mucus viscoelasticity. *Adv. Colloid Interface Sci.* **252**, 69–82. (doi:10.1016/j.cis.2017.12.005)
5. Kirch J, Schneider A, Abou B, Hopf A, Schaefer UF, Schneider M, Schall C, Wagner C, Lehr CM. 2012 Optical tweezers reveal relationship between microstructure and nanoparticle penetration of pulmonary mucus. *Proc. Natl Acad. Sci. USA* **109**, 18 355–18 360. (doi:10.1073/pnas.1214066109)
6. Philippe AM, Cipelletti L, Larobina D. 2017 Mucus as an arrested phase separation gel. *Macromolecules* **50**, 8221–8230. (doi:10.1021/acs.macromol.7b00842)
7. Gross A, Torge A, Schaefer UF, Schneider M, Lehr C-M, Wagner C. 2017 A foam model highlights the differences of the macro- and microrheology of respiratory horse mucus. *J. Mech. Behav. Biomed. Mater.* **71**, 216–222. (doi:10.1016/j.jmbbm.2017.03.009)
8. Puchelle E, Zahm JM, Duvivier C. 1983 Spinability of bronchial mucus. Relationship with viscoelasticity and mucous transport properties. *Biorheology* **20**, 239–249. (doi:10.3233/BIR-1983-20214)
9. Critchfield AS, Yao G, Jaishankar A, Friedlander RS, Lieleg O, Doyle PS, Mckinley G, House M, Ribbeck K. 2013 Cervical mucus properties stratify risk for preterm birth. *PLoS ONE* **8**, e69528. (doi:10.1371/journal.pone.0069528)
10. Vasquez PA, Forest MG. 2015 Complex fluids and soft structures in the human body. In *Complex fluids in biological systems* (ed. S Spagnolie), pp. 53–110. New York, NY: Springer. (doi:10.1007/978-1-4939-2065-5_2)
11. Vasquez ES, Bowser J, Swiderski C, Walters KB, Kundu S. 2014 Rheological characterization of mammalian lung mucus. *RSC Adv.* **4**, 34 780–34 783. (doi:10.1039/C4RA05055J)
12. Ewoldt RH, Clasen C, Hosoi AE, Mckinley GH. 2007 Rheological fingerprinting of gastropod pedal

mucus and synthetic complex fluids for biomimicking adhesive locomotion. *Soft Matter* **3**, 634–643. (doi:10.1039/b615546d)
13. Weigand WJ, Messmore A, Tu J, Morales-Sanz A, Blair DL, Deheyn DD, Urbach JS, Robertson-Anderson RM. 2017 Active microrheology determines scaledependent material properties of *Chaetopterus* mucus. *PLoS ONE* **12**, e0176732. (doi:10.1371/journal.pone.0176732)
14. Celli JP, Turner BS, Afdhal NH, Ewoldt RH, Mckinley GH, Bansil R, Erramilli S. 2007 Rheology of gastric mucin exhibits a pH-dependent sol-gel transition. *Biomacromolecules* **8**, 1580–1586. (doi:10.1021/bm0609691)
15. Wang YY, Lai SK, Ensign LM, Zhong W, Cone R, Hanes J. 2013 The microstructure and bulk rheology of human cervicovaginal mucus are remarkably resistant to changes in pH. *Biomacromolecules* **14**, 4429–4435. (doi:10.1021/bm401356q)
16. King M, Macklem PT. 1977 Rheological properties of microliter quantities of normal mucus. *J. Appl. Physiol. Respir. Environ. Exer. Physiol.* **42**, 797–802.
17. Schuster BS, Suk JS, Woodworth GF, Hanes J. 2013 Nanoparticle diffusion in respiratory mucus from humans without lung disease. *Biomaterials* **34**, 3439–3446. (doi:10.1016/j.biomaterials.2013.01.064)
18. Lai SK, Wang Y-Y, Wirtz D, Hanes J. 2009 Micro- and macrorheology of mucus. *Adv. Drug Deliv. Rev.* **61**, 86–100. (doi:10.1016/j.addr.2008.09.012)
19. Bokkasam H, Ernst M, Guenther M, Wagner C, Schaefer UF, Lehr C-M. 2016 Different macro- and micro-rheological properties of native porcine respiratory and intestinal mucus. *Int. J. Pharm.* **510**, 164–167. (doi:10.1016/j.ijpharm.2016.06.035)
20. Radiom M, Hénault R, Mani S, Iankovski AG, Norel X, Berret JF. 2021 Magnetic wire active microrheology of human respiratory mucus. *Soft Matter* **17**, 7585–7595. (doi:10.1039/D1SM00512J)
21. Meziu E, Koch M, Fleddermann J, Schwarzkopf K, Schneider M, Kraegeloh A. 2021 Visualization of the structure of native human pulmonary mucus. *Int. J. Pharm.* **597**, 120238. (doi:10.1016/j.ijpharm.2021.120238)
22. Ford AG, Cao XZ, Papanikolas MJ, Kato T, Boucher RC, Markovetz MR, Hill DB, Freeman R, Forest MG. 2021 Molecular dynamics simulations to explore the structure and rheological properties of normal and hyperconcentrated airway mucus. *Stud. Appl. Math.* **147**, 1369–1387. (doi:10.1111/sapm.12433)
23. Button B *et al.* 2018 Roles of mucus adhesion and cohesion in cough clearance. *Proc. Natl Acad. Sci. USA* **115**, 12 501–12 506. (doi:10.1073/pnas.1811787115)
24. Witten J, Samad T, Ribbeck K. 2019 Molecular characterization of mucus binding. *Biomacromolecules* **20**, 1505–1513. (doi:10.1021/acs.biomac.8b01467)
25. Jeffery P, Holgate S, Wenzel S. 2003 Methods for the assessment of endobronchial biopsies in clinical research: application to studies of pathogenesis and the effects of treatment. *Am. J. Respir. Crit. Care Med.* **168**, S1–S7. (doi:10.1164/rccm.200202-150WS)
26. Gras D *et al.* 2017 Epithelial ciliated beating cells essential for ex vivo ALI culture growth. *BMC Pulm. Med.* **17**, 80. (doi:10.1186/s12890-017-0423-5)
27. Gamez AS, Gras D, Petit A, Knabe L, Molinari N, Vachier I, Chanez P, Bourdin A. 2015 Supplementing defect in club cell secretory protein attenuates airway inflammation in COPD. *Chest* **147**, 1467–1476. (doi:10.1378/chest.14-1174)
28. Lafforgue O, Poncet S, Seyssiecq I, Favier J. 2017 Rheological characterization of macromolecular colloidal gels as simulant of bronchial mucus. *AIP Conf. Proc.* **1914**, 110003. (doi:10.1063/1.5016758)
29. Lafforgue O, Bouguerra N, Poncet S, Seyssiecq I, Favier J, Elkoun S. 2017 Thermo-physical properties of synthetic mucus for the study of airway clearance. *J. Biomed. Mater. Res. Part A* **105**, 3025–3033. (doi:10.1002/jbm.a.36161)
30. Ewoldt RH *et al.* 2015 Experimental challenges of shear rheology: how to avoid bad data. *Complex Fluids Biol. Systems* **7**, 3866–3871.
31. Tassieri M, Gibson GM, Evans RML, Yao AM, Warren R, Padgett MJ, Cooper JM. 2010 Measuring storage and loss moduli using optical tweezers: broadband microrheology. *Phys. Rev. E* **81**, 026308. (doi:10.1103/PhysRevE.81.026308)
32. Shundo A, Hori K, Penaloza DP, Tanaka K. 2013 Optical tweezers with fluorescence detection for temperature-dependent microrheological measurements. *Rev. Sci. Instrum.* **84**, 014013. (doi:10.1063/1.4789429)
33. Neuman KC, Block SM. 2004 Optical trapping. *Rev. Sci. Instrum.* **75**, 2787–2809. (doi:10.1063/1.1785844)
34. Jory M *et al.* 2019 Mucus microrheology measured on human bronchial epithelium culture. *Front. Phys.* **7**, 19. (doi:10.3389/fphy.2019.00019)
35. Berret JF, Porte G, Decruppe J-P. 1997 Inhomogeneous shear flows of wormlike micelles: a master dynamic phase diagram. *Phys. Rev. E* **55**, 1668–1676. (doi:10.1103/PhysRevE.55.1668)
36. Massiera G, Ramos L, Ligoure C. 2002 Role of the size distribution in the elasticity of entangled living polymer solutions. *Europhys. Lett.* **57**, 127–133. (doi:10.1209/epl/i2002-00551-4)
37. Payre B *et al.* 2018 A new HPF specimen carrier adapter for the use of high-pressure freezing with cryoscanning electron microscope: two applications: stearic acid organization in a hydroxypropyl methylcellulose matrix and mice myocardium. *J. Microsc.* **271**, 255–265. (doi:10.1111/jmi.12713)
38. Møller PCF, Mewis J, Bonn D. 2006 Yield stress and thixotropy: on the difficulty of measuring yield stresses in practice. *Soft Matter* **2**, 274–283. (doi:10.1039/b517840a)
39. Coussot P. 2014 Yield stress fluid flows: a review of experimental data. *J. Non-Newtonian Fluid Mech.* **211**, 31–49. (doi:10.1016/j.jnnfm.2014.05.006)
40. Oswald P. 2005 *Rhéophysique: ou comment coule la matière*. Paris, France: Belin.
41. Ewoldt RH, Hosoi AE, Mckinley GH. 2008 New measures for characterizing nonlinear viscoelasticity in large amplitude oscillatory shear. *J. Rheol.* **52**, 1427. (doi:10.1122/1.2970095)
42. Lafforgue O, Seyssiecq I, Poncet S, Favier J. 2018 Rheological properties of synthetic mucus for airway clearance. *J. Biomed. Mater. Res. Part A* **106**, 386–396. (doi:10.1002/jbm.a.36251)
43. Hill DB *et al.* 2014 A biophysical basis for mucus solids concentration as a candidate biomarker for airways disease. *PLoS ONE* **9**, e87681. (doi:10.1371/journal.pone.0087681)
44. Dawson M, Wirtz D, Hanes J. 2003 Enhanced viscoelasticity of human cystic fibrotic sputum correlates with increasing microheterogeneity in particle transport. *J. Biol. Chem.* **278**, 50 393–50 401. (doi:10.1074/jbc.M309026200)
45. Wagner CE, Turner BS, Rubinstein M, Mckinley GH, Ribbeck K. 2017 A rheological study of the association and dynamics of MUC5AC gels. *Biomacromolecules* **18**, 3654–3664. (doi:10.1021/acs.biomac.7b00809)
46. Johansson M, Tienthai P, Rodriguez-Martinez H. 2000 Histochemistry and ultrastructure of the intraluminal mucus in the sperm reservoir of the pig oviduct. *J. Reprod. Dev.* **46**, 183–192. (doi:10.1262/jrd.46.183)
47. Creton C, Leibler L. 1996 How does tack depend on time of contact and contact pressure? *J. Polym. Sci. B Polym. Phys.* **34**, 545–554. (doi:10.1002/(SICI)1099-0488(199602)34:3<545::AID-POLB13>3.0.CO;2-I)
48. Witten J *et al*. 2020 *HHS Public Access* **20**, 1505–1513.
49. Massiera G. 2022 Data from 'Mucus from human bronchial epithelial (HBE) cultures: rheology and adhesion across length scales'. Harvard Dataverse. (doi:10.7910/DVN/CPNW04)
50. Jory M, Donnarumma D, Blanc C, Bellouma K, Fort A, Vachier I, Casanellas L, Bourdin A, Massiera G. 2022 Mucus from human bronchial epithelial cultures: rheology and adhesion across length scales. Figshare. (doi:10.6084/m9.figshare.c.6189734)